

Meshless Time-Domain Method with Modified RPIM-Based Shape Functions for Electromagnetic Wave Propagation Simulation in Complex Shaped Domain^{*)}

Taku ITOH, Soichiro IKUNO and Hiroaki NAKAMURA¹⁾

Tokyo University of Technology, 1404-1 Katakura-machi, Hachioji, Tokyo 192-0982, Japan

¹⁾*National Institute for Fusion Science, 322-6 Oroshi-cho, Toki, Gifu 509-5292, Japan*

(Received 10 December 2013 / Accepted 27 March 2014)

To speed up electromagnetic wave propagation simulations using the meshless time-domain method (MTDM) in complex shaped domains, this paper presents a strategy for embedding the modified radial point interpolation method (MRPIM)-based shape functions to MTDM, while maintaining the stability of the simulations. Numerical experiments show that, by using the strategy with appropriate parameters, the stability of the simulations using MTDM with MRPIM-based shape functions (MRPIM-MTDM) is considerably improved. In addition, the approach of the amplification/damping rate to convergence in MRPIM-MTDM is almost the same as that in the conventional MTDM. Furthermore, the total computation time of MRPIM-MTDM is less than that of the conventional MTDM.

© 2014 The Japan Society of Plasma Science and Nuclear Fusion Research

Keywords: meshless time-domain method, meshless radial point interpolation method, electromagnetic propagation, waveguide bend, Maxwell equation

DOI: 10.1585/pfr.9.3401088

1. Introduction

In a large helical device (LHD), an electron cyclotron heating (ECH) system is used for plasma heating; electrical power generated by the gyrotron system is transmitted to the LHD via a long corrugated waveguide. However, the shape of the waveguide curvature and the theoretical transmission gain of electromagnetic wave propagation are not clear [1].

Finite-difference time-domain method (FDTD) has generally been applied to electromagnetic wave propagation simulations. FDTD can directly provide solutions of Maxwell equations. However, to apply FDTD in electromagnetic wave propagation simulations, the numerical domain must be divided into rectangular meshes, and it is difficult for an arbitrary-shaped domain to be accurately represented by rectangular meshes.

On the other hand, a meshless method based on the radial point interpolation method (RPIM) [3] has recently been applied to electromagnetic wave propagation simulations [2]. We refer to this as a meshless time-domain method (MTDM). MTDM does not require finite elements or meshes of a geometric structure, i.e., the node alignment of MTDM is more flexible than that of FDTD. Hence, MTDM can easily be applied in electromagnetic wave propagation simulations of complex shaped domains. However, the computational cost of MTDM tends to be larger than that of FDTD. This is because, in MTDM,

shape functions based on RPIM are usually employed; i.e., before starting the simulations, the i th shape function corresponding to the i th node has to be determined by solving linear systems constructed by using neighbor nodes ($i = 1, 2, \dots, N$), where N is the number of nodes. To apply MTDM to large-scale simulations, acceleration of MTDM may be indispensable.

Recently, a modified RPIM (MRPIM) [4] has been proposed. In MRPIM, the algorithm for determining the shape functions is rebuilt. By using MRPIM-based shape functions in MTDM, the computation efficiency of MTDM may be improved. However, if MRPIM-based shape functions are simply embedded in MTDM, the simulation using MTDM may be unstable [1].

The purpose of the present study is to speed up electromagnetic wave propagation simulations using MTDM in complex shaped domains. To this end, MRPIM is employed for generating shape functions for MTDM. In addition, to maintain the stability of simulations using MTDM, we present a strategy for embedding MRPIM-based shape functions in MTDM.

2. Meshless Time-Domain Method

To simulate electromagnetic wave propagation, we consider Maxwell equations in case of the two-dimensional (2D) TM mode described by

$$\varepsilon \frac{\partial E_z}{\partial t} = -\sigma E_z + \frac{\partial H_y}{\partial x} - \frac{\partial H_x}{\partial y}, \quad (1)$$

author's e-mail: taku@m.ieice.org

^{*)} This article is based on the presentation at the 23rd International Toki Conference (ITC23).

$$\mu \frac{\partial H_x}{\partial t} = -\frac{\partial E_z}{\partial y}, \quad (2)$$

$$\mu \frac{\partial H_y}{\partial t} = \frac{\partial E_z}{\partial x}, \quad (3)$$

where E_z denotes the z component of the electric field, and H_x and H_y denote the x and y components of the magnetic field, respectively. In addition, ε , σ , and μ denote the permittivity, electrical conductivity, and the magnetic permeability, respectively.

To discretize (1)–(3) by MTDM, nodes \mathbf{x}_i^E ($i = 1, 2, \dots, N^E$) for E_z and \mathbf{x}_i^H ($i = 1, 2, \dots, N^H$) for H_x and H_y are first aligned in a domain, where N^E denotes the number of nodes for E_z , and N^H denotes the number of nodes for H_x and H_y . In MTDM, the leapfrog method is employed to discretize the time-domain. The space domain is discretized by using shape functions based on meshless methods. The discretized forms of (1)–(3) are as follows [1, 2, 5]:

$$E_{z,i}^n = \frac{\left(\frac{\varepsilon}{\Delta t} - \frac{\sigma}{2} \right) E_{z,i}^{n-1} + \sum_{j=1}^{N^H} \left(H_{y,j}^{n-\frac{1}{2}} \frac{\partial \phi_{j,i}^H}{\partial x} - H_{x,j}^{n-\frac{1}{2}} \frac{\partial \phi_{j,i}^H}{\partial y} \right)}{\left(\frac{\varepsilon}{\Delta t} + \frac{\sigma}{2} \right)}, \quad (4)$$

$$H_{x,i}^{n+\frac{1}{2}} = H_{x,i}^{n-\frac{1}{2}} - \frac{\Delta t}{\mu} \sum_{j=1}^{N^E} E_{z,j}^n \frac{\partial \phi_{j,i}^E}{\partial y}, \quad (5)$$

$$H_{y,i}^{n+\frac{1}{2}} = H_{y,i}^{n-\frac{1}{2}} + \frac{\Delta t}{\mu} \sum_{j=1}^{N^E} E_{z,j}^n \frac{\partial \phi_{j,i}^E}{\partial x}, \quad (6)$$

where n is the time step, $E_{z,i}^n \equiv E_z^n(\mathbf{x}_i^E)$, $H_{x,i}^{n+\frac{1}{2}} \equiv H_x^{n+\frac{1}{2}}(\mathbf{x}_i^H)$, and $H_{y,i}^{n+\frac{1}{2}} \equiv H_y^{n+\frac{1}{2}}(\mathbf{x}_i^H)$. In addition, $\phi_j^E(\mathbf{x})$ and $\phi_j^H(\mathbf{x})$ denote the shape functions corresponding to \mathbf{x}_j^E ($j = 1, 2, \dots, N^E$) and \mathbf{x}_j^H ($j = 1, 2, \dots, N^H$), respectively.

3. Shape Functions for MTDM

By using MTDM, E_z , H_x , and H_y in (1)–(3) are discretized by shape functions based on meshless methods. Note that the shape functions $\phi_j^E(\mathbf{x})$ and $\phi_j^H(\mathbf{x})$ in (4)–(6) are similarly determined. Hence, in this section, we do not use E and H as superscripts.

In MTDM, it is assumed that the shape functions satisfy a property, $\phi_i(\mathbf{x}_j) = \delta_{ij}$, where δ_{ij} is the Kronecker delta [3]. In the following section, we describe the original and modified RPIM-based shape functions, since both shape functions satisfy the above property.

3.1 Original RPIM-based shape functions

First, the nodes, $\mathbf{x}_1, \mathbf{x}_2, \dots, \mathbf{x}_N$, together with the radial basis functions (RBFs), $w_1(\mathbf{x}), w_2(\mathbf{x}), \dots, w_N(\mathbf{x})$, on each of the nodes are assigned in the domain Ω and on the boundary $\partial\Omega$, where N is the number of nodes, and $w_i(\mathbf{x}) \equiv w(|\mathbf{x} - \mathbf{x}_i|)$ ($i = 1, 2, \dots, N$). In RPIM, it is assumed that a function $u(\mathbf{x})$ can be expanded as

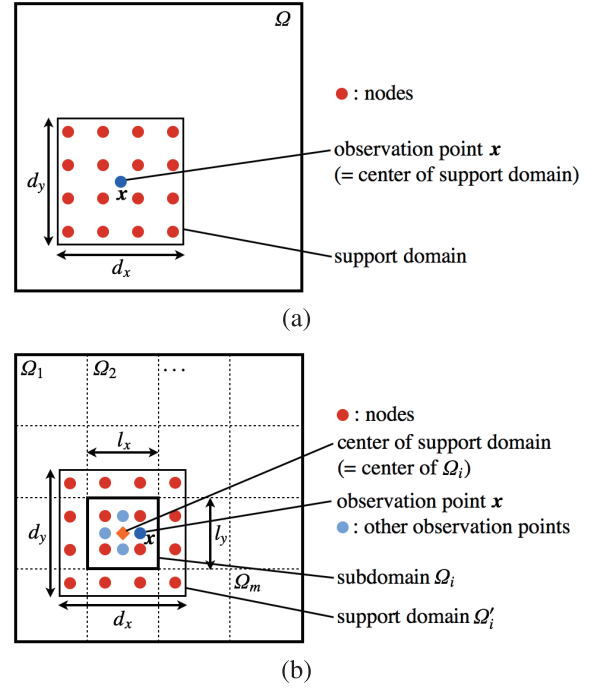


Fig. 1 Support domains for (a) original RPIM-based shape function and (b) modified RPIM-based shape function.

$$u(\mathbf{x}) = \sum_{i=1}^N u_i \phi_i(\mathbf{x}), \quad (7)$$

where u_i is a coefficient, and $\phi_i(\mathbf{x})$ denotes the shape function corresponding to the i th node \mathbf{x}_i ($i = 1, 2, \dots, N$). Note that the i th shape function is defined by using a support domain centered at an observation point \mathbf{x} . A schematic of the rectangular support domain is illustrated in Fig. 1 (a).

Inside the support domain, the shape functions $\phi_1(\mathbf{x}), \phi_2(\mathbf{x}), \dots, \phi_{N_s}(\mathbf{x})$ corresponding to $\mathbf{x}_1, \mathbf{x}_2, \dots, \mathbf{x}_{N_s}$ are determined by solving the linear systems as follows [3]:

$$G\boldsymbol{\phi}(\mathbf{x}) = \mathbf{b}(\mathbf{x}), \quad (8)$$

where $\mathbf{x}_1, \mathbf{x}_2, \dots, \mathbf{x}_{N_s}$ are nodes contained in the support domain, N_s is the number of nodes inside the support,

$$G \equiv \begin{bmatrix} W & P \\ P^T & O \end{bmatrix}, \quad \mathbf{b}(\mathbf{x}) \equiv \begin{bmatrix} \mathbf{w}(\mathbf{x}) \\ \mathbf{p}(\mathbf{x}) \end{bmatrix}, \quad (9)$$

$$W \equiv [\mathbf{w}(\mathbf{x}_1), \mathbf{w}(\mathbf{x}_2), \dots, \mathbf{w}(\mathbf{x}_{N_s})]^T,$$

$$P \equiv [\mathbf{p}(\mathbf{x}_1), \mathbf{p}(\mathbf{x}_2), \dots, \mathbf{p}(\mathbf{x}_{N_s})]^T,$$

$$\boldsymbol{\phi}(\mathbf{x}) \equiv [\phi_1(\mathbf{x}), \phi_2(\mathbf{x}), \dots, \phi_{N_s}(\mathbf{x})]^T,$$

$$\mathbf{w}(\mathbf{x}) \equiv [w_1(\mathbf{x}), w_2(\mathbf{x}), \dots, w_{N_s}(\mathbf{x})]^T, \text{ and}$$

$$\mathbf{p}(\mathbf{x}) \equiv [p_1(\mathbf{x}), p_2(\mathbf{x}), \dots, p_M(\mathbf{x})]^T.$$

Similarly, partial derivatives of $\boldsymbol{\phi}(\mathbf{x})$ with respect to x and y are, respectively, determined by solving the linear systems as follows:

$$G \frac{\partial \boldsymbol{\phi}}{\partial x}(\mathbf{x}) = \frac{\partial \mathbf{b}}{\partial x}(\mathbf{x}), \text{ and } G \frac{\partial \boldsymbol{\phi}}{\partial y}(\mathbf{x}) = \frac{\partial \mathbf{b}}{\partial y}(\mathbf{x}). \quad (10)$$

In this study, for the 2D case, we adopt $M = 3$; i.e., $\mathbf{p}(\mathbf{x}) = [1, x, y]^T$, whose components are coefficients of a first-degree polynomial.

3.2 Modified RPIM-based shape functions

In MRPIM, the coefficient matrix G in (8) and (10) is independent of the observation point \mathbf{x} ; instead, G is constructed for each subdomain. Figure 1 (b) shows an example of rectangular subdomains $\Omega_1, \Omega_2, \dots, \Omega_m$ generated by dividing the domain Ω . This figure also shows a support domain Ω'_i for the i th subdomain Ω_i . Note that Ω'_i is not determined from the observation point \mathbf{x} but from the center of Ω_i [4].

4. Strategy for Embedding MRPIM-Based Shape Functions in MTDM

In MRPIM, the subdomains, $\Omega_1, \Omega_2, \dots, \Omega_m$ and their support domains have to be determined. For electromagnetic wave propagation simulations by MTDM with MRPIM-based shape functions in waveguide bends, we choose rectangular subdomains of the same size, since we suppose that nodes \mathbf{x}_i^E ($i = 1, 2, \dots, N^E$) and \mathbf{x}_i^H ($i = 1, 2, \dots, N^H$) are uniformly aligned inside the waveguide. Figure 2 shows a schematic of the rectangular subdomains.

In Ω_i , to determine the support domain Ω'_i , we present a strategy for adjusting the number N_s of nodes contained in Ω'_i so that $N_s \in [N_{\min}, N_{\max}]$ is satisfied as much as possible. Here, N_{\min} and N_{\max} are user-specified parameters that denote the minimum and maximum numbers of nodes contained in Ω'_i . This is because if Ω'_i does not contain sufficient nodes, unexpected evaluation results for shape functions may be obtained on an observation point \mathbf{x} in Ω_i . In addition, N_s influences the size of the matrix G , i.e., if N_s is too large, the computational cost for solving (8) and (10) significantly increases. Furthermore, without the strategy, simulations using MTDM with MRPIM-based shape functions may be unstable, as shown in Section 5. The strategy is represented by the following C-like pseudo-code that is based on an algorithm given in [6].

```

dx = βxlx;   dy = βyly;   k = 0;
do{
    Xs = searchNeighborNodes(Ns, c, dx, dy);
    if(Ns < Nmin){ dx += βxElx;   dy += βyEly; }
    else if(Ns > Nmax){ dx -= βxRlx;   dy -= βyRly; }
    ++k;
}while(Ns ∉ [Nmin, Nmax] && k < kmax);
    
```

Here, d_x and d_y denote the x - and y -length of Ω'_i , respectively, and l_x and l_y denote the x - and y -length of Ω_i , respectively. In addition, $\beta_x, \beta_y, \beta_x^E, \beta_y^E, \beta_x^R, \beta_y^R$ and k_{\max} are user-specified parameters. In particular, β_x and β_y are set for determining the initial lengths of d_x and d_y , respectively; β_x^E and β_y^E are set for enlarging d_x and d_y , respectively; and β_x^R and β_y^R are set for reducing d_x and d_y , respectively. Note that k_{\max} is set for determining the maximum number of iterations, since satisfying $N_s \in [N_{\min}, N_{\max}]$ is sometimes difficult, depending on the node alignment.

In the function “searchNeighborNodes,” nodes contained in a rectangular domain Ω'_i of center \mathbf{c} , x -length d_x and y -length d_y are searched, and the nodes are returned to

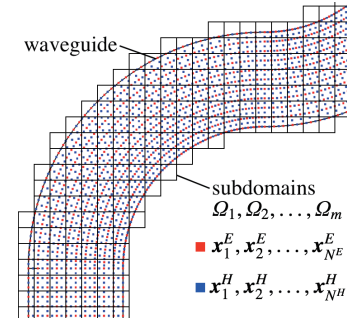


Fig. 2 Schematic of rectangular subdomains for a waveguide bend.

\mathcal{X}_s . In addition, the number N_s of nodes \mathcal{X}_s is updated in the function. Note that the center \mathbf{c} of Ω'_i coincides with the center of Ω_i . After the do-while loop, we set $\Omega'_i = \hat{\Omega}'_i$.

5. Numerical Experiments

In this section, numerical experiments are conducted to investigate the performance of MTDM with MRPIM-based shape functions for a 2D electromagnetic wave propagation simulation in the waveguide bend illustrated in Fig. 3 (a). In the figure, we set $w = 0.3$ m, $h = 1.2$ m, and $R = 0.45$ m. In addition, in the simulation, we assume that the wave source is a sine wave whose amplitude, frequency, and speed are 1.0 V/m, 1.0×10^9 Hz, and 299792458 m/s, respectively. Furthermore, to satisfy the Courant condition for the 2D MTDM [5], $\Delta t = 0.6 \min|\mathbf{x}_i^H - \mathbf{x}_j^H|/c$ s ($i, j = 1, 2, \dots, N^H, i \neq j$), where c is the speed of light.

In Fig. 3 (a), \mathbf{x}_i^E and \mathbf{x}_j^H are represented as red squares and blue triangles, respectively ($i = 1, 2, \dots, N^E, j = 1, 2, \dots, N^H$). In addition, the node alignment is based on the staggered mesh that is employed in the standard FDTD. This is because the simulation may become unstable if the node alignment is inappropriate [5]. As boundary conditions, the perfectly matched layer (PML) and the perfect electric conductor (PEC) are employed. PMLs are imposed at the waveguide edges, and PECs are imposed on the waveguide sides, as shown in Fig. 3 (a). Note that these boundary conditions in MTDM can be imposed in the same manner as in FDTD (see [7] for more details).

To generate shape functions for MTDM, we adopt a reciprocal multi quadric (RMQ):

$$w_i(\mathbf{x}) = \left(\frac{|\mathbf{x} - \mathbf{x}_i|^2}{d_i^2} + \alpha^2 \right)^{-\frac{1}{2}}, \quad (11)$$

as the RBF in (9), where $d_i = \sqrt{d_x^2 + d_y^2}$, and α is a user-specified parameter; we set $\alpha = 0.1$. In addition, we set $l_x = 1.3\Delta x$ m, $l_y = 1.3\Delta y$ m, $\beta_x = \beta_y = 3.0$, $\beta_x^E = \beta_y^E = 0.11$, $\beta_x^R = \beta_y^R = 0.07$, and $k_{\max} = 100$.

Computations are performed on a computer equipped with a 2.66 GHz Intel Core i7 920 processor, 24 GB RAM, Ubuntu Linux ver. 12.10, and g++ ver. 4.7.2 with double-

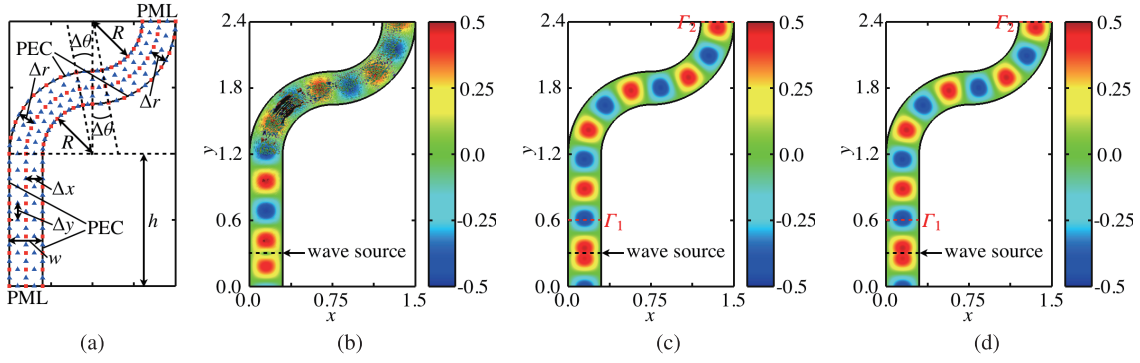


Fig. 3 (a) Schematic of the waveguide bend employed in the numerical experiments. In this figure, \mathbf{x}_i^E and \mathbf{x}_i^H are represented as red squares and blue triangles, respectively. (b) Distribution of E_z obtained from MRPIM-MTDM without the strategy for adjusting N_s ($t = 54000\Delta t$, $N = 96165$). Black regions correspond to an inappropriate value for E_z . (c) Distribution of E_z obtained from RPIM-MTDM ($t = 70000\Delta t$, $N = 302645$). (d) Distribution of E_z obtained from MRPIM-MTDM ($t = 70000\Delta t$, $N = 302645$).

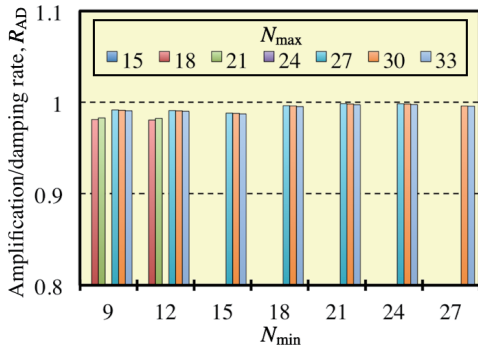


Fig. 4 Dependence of the amplification/damping rate R_{AD} on N_{min} and N_{max} for $N = 211715$.

precision arithmetic. In the following, RPIM-MTDM and MRPIM-MTDM denote MTDMs with original and modified RPIM-based shape functions, respectively.

Figure 3 (b) shows the distribution of E_z obtained from MRPIM-MTDM without the strategy for adjusting N_s . The distribution is observed in $t = 54000\Delta t$ s. The parameters for determining N are fixed at $\Delta x = \Delta y = \Delta r = 0.006$ m and $\Delta\theta = \pi/400$, thus $N = 96165$, where $N = N^E + N^H$. Note that N^E and N^H include the number of nodes contained in PML regions, and the number of layers for each PML region is 16. The parameters for support domains are fixed at $d_x = 1.5l_x$ m and $d_y = 1.5l_y$ m, i.e., d_x and d_y for all support domains are all the same. In Fig. 3 (b), the black parts denote regions in which E_z has inappropriate values. These black parts appear from around $t = 50000\Delta t$ s, and E_z subsequently diverged. These results suggest that the simulation becomes unstable when d_x and d_y are constant for all support domains. Hence, a strategy for adjusting N_s is necessary for embedding MRPIM in MTDM.

To determine appropriate values for N_{min} and N_{max} , the dependence of the amplification/damping rate R_{AD} on N_{min} and N_{max} is shown in Fig. 4. The parameters are fixed at $\Delta x = \Delta y = \Delta r = 0.004$ m and $\Delta\theta = \pi/600$, thus $N = 211715$. Although a pair of N_{min} and N_{max} for generating $\phi_i^E(\mathbf{x})$ ($i = 1, 2, \dots, N^E$) and $\phi_i^H(\mathbf{x})$ ($i = 1, 2, \dots, N^H$) can

be set separately, the same pair is used for generating $\phi_i^E(\mathbf{x})$ and $\phi_i^H(\mathbf{x})$. Note that the subdomains for $\phi_i^E(\mathbf{x})$ and for $\phi_i^H(\mathbf{x})$ are exactly the same. However, the support domains for $\phi_i^E(\mathbf{x})$ and for $\phi_i^H(\mathbf{x})$ are not the same, since $\phi_i^E(\mathbf{x})$ and $\phi_j^H(\mathbf{x})$ are separately generated, although the same pair of N_{min} and N_{max} is chosen. Here, the amplification/damping rate R_{AD} is defined as follows:

$$R_{AD} \equiv \left\langle \int_{\Gamma_2} |\mathbf{E} \times \mathbf{H}| d\ell \right\rangle_t \left/ \left\langle \int_{\Gamma_1} |\mathbf{E} \times \mathbf{H}| d\ell \right\rangle_t \right. . \quad (12)$$

In (12), to calculate R_{AD} , the y -coordinate of Γ_1 and that of Γ_2 are set to 0.6 and 2.4, respectively (see Figs. 3 (c) and 3 (d)). In Fig. 4, we attempted to calculate R_{AD} for all cases that satisfy $N_{min} < N_{max}$. However, for some pairs of N_{min} and N_{max} , R_{AD} could not be calculated, since the simulations using these pairs were unstable. Note that R_{AD} for these pairs are not shown in Fig. 4. Especially for $N_{max} = 15$ and 24, the simulations were always unstable. For this reason, there is no bar for $N_{max} = 15$ and 24 in Fig. 4. The figure shows that, when N_{min} is relatively small, R_{AD} cannot be calculated occasionally. In addition, for $N_{max} \geq 27$, R_{AD} can be calculated for all cases. Based on these results, we fixed $N_{min} = 21$ and $N_{min} = 27$.

For the following, electromagnetic wave propagation is simulated by using the above fixed values for N_{min} and N_{max} . Figures 3 (c) and 3 (d) show distributions of E_z obtained from RPIM-MTDM and MRPIM-MTDM, respectively. Both distributions were observed at $t = 70000\Delta t$ s. Parameters are fixed at $\Delta x = \Delta y = \Delta r = 1/300$ (m) and $\Delta\theta = \pi/720$, thus $N = 302645$. It must be noted here that, when MRPIM-MTDM without the strategy for adjusting N_s is applied to a simulation with the same parameters, the simulation becomes unstable from around $t = 1400\Delta t$. Hence, by using the strategy with appropriate parameters, the stability of electromagnetic wave propagation simulations using the MRPIM-MTDM is considerably improved. For the quantitative comparisons between the two distributions, a maximum error $\varepsilon_{max} \equiv \max_{i=1}^{N^E} |E_{z,i}^{RPIM} - E_{z,i}^{MRPIM}| / \max |E_z|$ and an average error

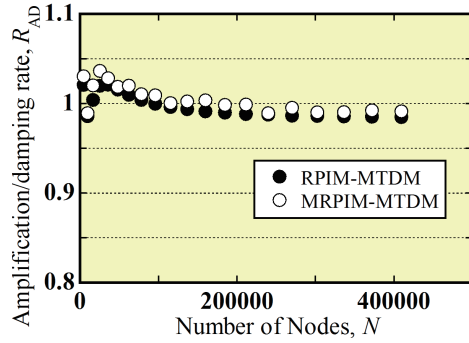


Fig. 5 Dependence of the amplification/damping rate R_{AD} on N .

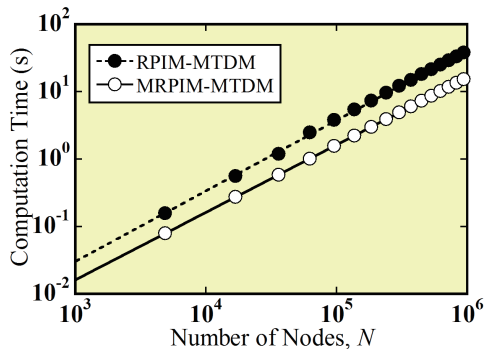


Fig. 6 Computation time dependence for determining the partial derivatives of $\phi_i^E(x)$ at x_j^E and those of $\phi_j^H(x)$ at x_i^E on N ($i = 1, 2, \dots, N^E, j = 1, 2, \dots, N^H$).

$\varepsilon_{avg} \equiv \sum_{i=1}^{N^E} |E_{z,i}^{RPIM} - E_{z,i}^{MRPIM}| / (N^E \max |E_z|)$ are calculated, where $E_{z,i}^{RPIM}$ and $E_{z,i}^{MRPIM}$ denote $E_z(x_i^E)$ obtained from RPIM-MTDM and MRPIM-MTDM, respectively. In addition, $\max |E_z| = 1.0$, since the wave source is a sine wave whose amplitude is 1.0 V/m. The calculated errors are $\varepsilon_{max} = 1.72 \times 10^{-2}$ and $\varepsilon_{avg} = 1.68 \times 10^{-3}$. Hence, although the two distributions in Figs. 3 (c) and 3 (d) are visually almost the same, the difference between $E_{z,i}^{RPIM}$ and $E_{z,i}^{MRPIM}$ is up to about 1.72% and on average it is about 0.168%.

To investigate the convergence of R_{AD} in both methods, R_{AD} is plotted as a function of N , as shown in Fig. 5. The figure shows that there is no obvious difference between R_{AD} of the two methods. In addition, from around $N = 100000$, $R_{AD} \approx 1.0$ in both methods. In the methods, R_{AD} essentially converged to a value that is slightly less than 1.0. Since $R_{AD} < 1$ at convergence, the electromagnetic wave is slightly damped in both methods. We consider that this damping is caused by wave reflections in the waveguide bend.

Finally, we investigate the computation time of both methods. We first focus on the iteration of (4)–(6). For 30000 iterations and $N = 96165$, the computation times for RPIM-MTDM and MRPIM-MTDM are about 467.7 s and 410.1 s, respectively. For 30000 iterations and $N = 302645$, the computation times for RPIM-MTDM and MRPIM-MTDM are about 1454.3 s and 1282.6 s, respectively. From these results, we conclude that MRPIM-

MTDM is slightly faster than RPIM-MTDM. Next, we focus on the process for determining $\frac{\partial \phi_j^E}{\partial x}(x_j^H)$, $\frac{\partial \phi_j^E}{\partial y}(x_j^H)$, $\frac{\partial \phi_i^H}{\partial x}(x_i^E)$ and $\frac{\partial \phi_i^H}{\partial y}(x_i^E)$ ($i = 1, 2, \dots, N^E, j = 1, 2, \dots, N^H$). This process is required once before starting the iterations of (4)–(6). For both methods, the computation time dependence for this process on N is shown in Fig. 6. The figure shows that, in all cases, the computation time for MRPIM-MTDM is about 2.38 times less than that for RPIM-MTDM. Therefore we conclude that the total computation time for MRPIM-MTDM is less than that for RPIM-MTDM. Especially when N is large, the difference in the computation times increases for the two methods.

6. Conclusion

To speed up electromagnetic wave propagation simulations using the MTDM in complex shaped domains, a strategy for embedding the modified radial point interpolation method (MRPIM)-based shape functions in MTDM while maintaining the stability of the simulations has been presented. In numerical experiments, the performance of MRPIM-MTDM has been investigated and compared with that of MTDM with the RPIM-based shape functions (RPIM-MTDM). Conclusions obtained in the present study are summarized as follows:

1. By using the strategy for adjusting N_s together with appropriate parameters, the stability of electromagnetic wave propagation simulations using the MRPIM-MTDM is considerably improved.
2. The approach to convergence of R_{AD} in MRPIM-MTDM is almost the same as that in RPIM-MTDM.
3. The total computation time for MRPIM-MTDM is less than that for RPIM-MTDM.

In a future study, details for damping the electromagnetic wave will be investigated. In addition, MRPIM-MTDM will be applied to larger-scale problems including three-dimensional cases.

Acknowledgment

This work was partially supported by JSPS KAKENHI Grant Number 24700053. In addition, this work was supported in part by NIFS Collaboration Research Program (NIFS13KNTS025 and NIFS13KNXN267).

- [1] S. Ikuno, Y. Fujita, T. Itoh, S. Nakata, H. Nakamura and A. Kamitani, *Plasma Fusion Res.* **7**, 2406044 (2012).
- [2] T. Kaufmann, C. Engström, C. Fumeaux and R. Vahldieck, *IEEE Trans. Microw. Theory Tech.* **58**, 3399 (2010).
- [3] J.G. Wang and G.R. Liu, *Int. J. Numer. Methods Eng.* **54**, 1623 (2002).
- [4] S. Nakata, *JNAIAM* **4**, 193 (2009).
- [5] T. Itoh, S. Ikuno, Y. Fujita and H. Nakamura, *Plasma Fusion Res.* **8**, 2401101 (2013).
- [6] I. Tobor, P. Reuter and C. Schlick, *WSCG* **12**, 467 (2004).
- [7] S. Ikuno, Y. Fujita, T. Itoh, S. Nakata and A. Kamitani, *Proc. of 15th IGTE Symposium 2012*, 53 (2012).